Chinese Chemical Letters 32 (2021) 604–608

Contents lists available at ScienceDirect

Chinese Chemical Letters

journal homepage: www.elsevier.com/locate/cclet

Communication

Two 2D uranyl coordination complexes showing effective photocatalytic degradation of Rhodamine B and mechanism study

Xiaolan Tong[a,b], Shan Wang[a], Jun Zuo[a], Yingchong Ge[a], Qiang Gao[c], Suijun Liu[d], Jianhua Ding[a], Fen Liu[a], Jianqiang Luo[a,b,*], Jianbo Xiong[a,b,*]

[a] State Key Laboratory of Nuclear Resources and Environment, School of Chemistry, Biology and Materials Science, East China University of Technology, Nanchang 330013, China
[b] Jiangxi Province Key Laboratory of Synthetic Chemistry, East China University of Technology, Nanchang 330013, China
[c] School of Environmental and Chemical Engineering, Jiangsu University of Science and Technology, Zhenjiang 212003, China
[d] School of Chemistry and Chemical Engineering, Jiangxi University of Science and Technology, Ganzhou 341000, China

ARTICLE INFO

Article history:
Received 4 November 2020
Received in revised form 18 November 2020
Accepted 23 November 2020
Available online 30 November 2020

Keywords:
Uranyl-organic frameworks
Photocatalytic degradation
Coordination complexes
Photocurrent
Mechanism

ABSTRACT

Two new hydrostable two-dimensional (2D) uranyl coordination complexes $[(UO_2)_5(\mu_3\text{-}O)_2(nbca)_2]\cdot 7H_2O$ (**1**) and $[(UO_2)_3(nbca)_2(H_2O)_3]\cdot 2H_2O$ (**2**) (H_3nbca = 5-nitro-1,2,3-benzenetricarboxylic acid) were hydrothermal synthesized. Single-crystal structural refinements reveal that both of the two complexes were formed by the packing of 2D uranyl coordination sheets *via* the hydrogen bonds. The nbca ligand coordinating to the uranyl polyhedron centers constructed the 2D sheets. There are UO_8 hexagonal bipyramids and UO_7 pentagonal bipyramids in **1** while only UO_7 pentagonal bipyramids in **2**. Photocatalytic degradation of rhodamine B (RhB) in aqueous solution was studied. Complex **2** possesses better performance than **1** with 96.2 % of the RhB was degraded in only 60 min. Mechanism studies reveal that the dissolved oxygens are essential to the RhB degradation. The photocurrent density of **2** is more stable than that of **1**, which indicating the stronger ability to separate photoexcited electrons and hole pairs of **2**.

Research on the uranium firstly boosted in the 20th century for the famous Manhattan Project [1]. In order to improve the enrichment of the isotopic ^{235}U as the raw material of the nuclear power, the uranium organometallic chemistry was extensively studied [1,2]. More recently, uranium is experiencing a renaissance for the design and construction of uranyl-organic frameworks (UOFs) [3–6]. The UOFs have intrigued considerable interests for they integrated both merits of the organic ligands and inorganic metals, supporting possibilities for versatile architectures and potential applications in wide functional fields including photocatalysis [7,8], luminescence [9,10], ion recognition [11]. Hexavalent uranium usually exists in the form of linear UO_2^{2+} dication with two "yl" oxo atoms coordinated along the axial direction, while the equatorial plane can accommodate four to six coordinate atoms thus demonstrating diverse polyhedrons from tetragonal, pentagonal, to hexagonal bipyramidal geometries [8,12]. These various polyhedron centers can be further conjugated by the organic ligands form abundant structures with different dimensionalities including zero-dimensional (0D) molecular clusters, one-dimensional (1D) molecular chains [13,14], two-dimensional (2D) layers [15] and three-dimensional (3D) frameworks [16,17]. In addition, ^{238}U take 99.28% abundance of the uranium and only exhibits an extremely low radioactive activity with 3.361×10^{-7} Ci/g for its long half-life time [11]. The structural diversities and radioactive safety support the feasibility for the design and synthesis of functional uranyl-based materials.

Efficient removal of the toxic and hard degraded organic pollutants in water has become a hotspot for the environmental and ecological importance [18–20]. Photocatalytic degradation is identified to be a useful method to handle the organic pollutants in water for the solar power is adequate and low-cost [21]. Traditional metal oxide semiconductors (like TiO_2) produce electron-hole (e^--h^+) pairs under irradiation of UV light which can degrade various kinds of refractory organic pollutants. However, the UV light only make up of 5% of the solar light. Exploiting novel materials to fully using the visible light (account for 45% of the solar light) is more significant to the future large-scale application [18].

* Corresponding authors at: State Key Laboratory of Nuclear Resources and Environment, School of Chemistry, Biology and Materials Science, East China University of Technology, Nanchang 330013, China.
E-mail addresses: luojianqiang@163.com (J. Luo), 201960278@ecut.edu.cn, xiongjianbo1210@163.com (J. Xiong).

https://doi.org/10.1016/j.cclet.2020.11.044
1001-8417/

It is well known that the uranyl ion can generate a long-life standard oxidation potential of +2.6 V [22] and are proved effective towards many type organic pollutants [23]. The dispersion of uranyl ions in the reaction systems may limit its application, while immobilization the uranyl ions into the stable uranyl-organic frameworks can overcome this drawback and may even enhance the photocatalytic performance [24,25]. For example, Sun *et al.* [24] reported two-dimensional and three-dimensional uranyl coordination polymers constructed from (2-carboxyethyl)(phenyl)-phosphinic acid, the effective photocatalytic degradation of RhB was studied. Zheng *et al.* [25] reported six UOFs structures from naphthalene dicarboxylic acid and their photocatalytic degradation of tetracycline, density functional theory (DFT) calculations were performed to understand the photocatalytic properties. While the studies of photocatalytic mechanism combining anaerobic experiments and photocurrent test are rare.

Herein, we synthesized two new 2D uranyl coordination complexes using polycarboxylates ligand 5-nitro-1,2,3-benzenetricarboxylic acid under the guidance of HSAB (hard/soft acid/base) theory (Scheme 1) [2]. The photocatalytic degradation of RhB by the two complexes was studied. Contrast experiment under anaerobic condition and photocurrent test were performed to reveal the photocatalytic mechanism. The single-crystal structures, phase purities, thermostability and luminescence were also demonstrated.

X-ray single crystal structural analysis reveals that complex **1** crystallized in triclinic crystal system with *P*-1 space group. Every asymmetric unit consists of one crystalographically independent $nbca^{3-}$ ligand, two and a half UO_2^{2+}, one μ_3-O atom and three and a half free water molecules (Fig. 1a) [26]. There are two kinds of coordination configurations for the uranyl centers in complex **1**. As shown in Fig. 1, the U1 center adopts eight-coordinated dodecahedron geometry with four μ_1-η^2 oxygens from two different nbca ligands and two μ_3-O atoms (O9) bound at the equatorial position. The U1 center is seated on a symcenter with the U1=O bond length being of 1.772 Å and the O=U1=O angle being of 180° (Table S2 in Supporting information). The U=O bond lengths on the equatorial plane are range in the value of 2.235–2.593 Å. The U2 and U3 both take seven-coordinated decanedron configuration with five oxygens at the equatorial position consists of three μ_3-O atoms and two carboxyl oxygens from different nbca ligands. The U=O bond lengths and O=U=O bond angles for U2 centers are 1.783 Å, 1.787 Å and 176.3°, these values for U3 centers are 1.772 Å, 1.779 Å and 176.5°, respectively. The U—O bond lengths at the equatorial position for U2 and U3 are in the range of 2.241–2.546 Å (Table S2). Both the bond lengths and angles embraced on the uranyl centers are in good agreement to the reported uranyl complexes [9,25]. Every nbca ligand in complex **1** coordinated to five uranyl centers with one μ_2-η^1:η^1 carboxyl group bound to two uranyl centers, one μ_3-η^2:η^2 carboxyl group bound to three uranyl centers and one η^1 carboxyl group (Fig. S3 in Supporting information). The U1 dodecahedron connected to four decanedron uranyl centers *via* edge-sharing oxygens forming close connected five uranyl center unit structure (Fig. 1b). The five membered uranyl unit further connected the adjacent uranyl unit *via* two edge-sharing μ_3-O atoms and two μ_2-η^1:η^1 carboxyl groups forming one-dimensional chain structure along [010] direction. The uranyl and oxygen chains connected by the inter-chain nbca ligands formed two-dimensional (2D) sheer (Fig. 1c). There are abundant free water molecules imbedded among the interlayers, which separate the 2D sheers with interlayer distance being of 7.52 Å (Fig. 1d). The free water molecules imbedded in the interlayers and the vertical oxygens from the uranyl centers on the 2D sheer contribute together to the formation of hydrogen bonds (Fig. 1e). The distances of the hydrogen to the acceptor (H···A) are varied from 2.14 Å to 2.54 Å (Fig. 1e and Table S3 in Supporting information). The detail information of the hydrogen bonds is listed in Table S2. The accessible void space is only 4.3% (42.9 $Å^3$ out of 1002.8 $Å^3$, calculated by PLATON) due to the close packing of the 2D sheer and the padding of the water [3].

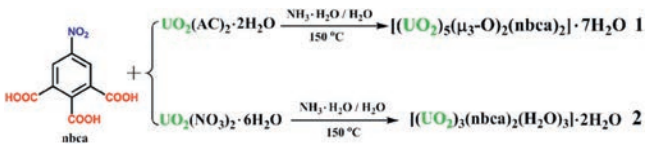

Scheme 1. Preparation of the coordination complexes **1** and **2**.

Different to **1**, complex **2** crystallized in monoclinic crystal system of $P2_1/c$ space group. The crystallographic asymmetric unit consists of three uranyl ions, two $nbca^{3-}$ ligands, three coordinated water and two free water molecules (Fig. 2a). Though all of the uranyl centers take seven-coordinated mode with the uranyl seated in the decanedron center, there are difference in the atoms which constructed the polyhedron geometry. U3 bind two η^1 oxygens and three coordinated water molecules in the equatorial plane. The U3=O bond lengths are 1.746 Å and 1.773 Å, and the O=U3=O bond angle is 179.3°. The U—O bond lengths in the equatorial plane are range from 2.321 Å to 2.494 Å (Table S2). These bond lengths and angles are common to the other reported majority uranyl compounds [8,27]. U1 and U2 connected by two η^2 oxygens forming edge-sharing double decanedron geometry. The nbca ligand linking four uranyl ions with the three carboxyl groups in μ_2-η^1:η^1 and μ_2-η^2:η^0 mode, respectively (Fig. S3). Specially, the edge-sharing double decanedron centers jointed *via* the adjacent μ_2-η^1:η^1 carboxyl groups resulting in a zigzag chain structure along [001] direction. The decanedron U3 center further connected the edge-sharing double uranyl center chains forming two-dimensional sheet on *ac* plane (Fig. 2b). Similar to **1**, abundant free water included among the gap between the 2D layers. The layer to layer distance of **2** is longer than that of **1**, with value of 8.44 Å (Fig. 2c). The interbeded free water molecules together with the neighbouring oxygens form uranyl and nitryl contribute to form hydrogen bonds between the layers [28]. In addition, the coordinated water molecules although connected the adjacent uranyl *via* hydrogen bonds. The distances between the donated hydrogen and accepted oxygens are varied from 1.74 Å to 2.58 Å (Fig. 2d and Table S3). These interbeded hydrogen bonds contribute to the packing of the 2D layers forming three-dimensional supramolecular assembly. The calculated result reveals that the unit cell contains no residual solvent accessible void due to the densely packed spatial structure.

In order to further investigate the crystalline phase purity, structural information and thermostability, powder X-ray diffraction, infrared spectroscopy (IR) and thermogravimetric analysis (TGA) measurements were performed. As shown in Fig. S4 (Supporting informaton), the measured PXRD pattern fitted well to their simulated spectrum from crystal information file (cif). The IR spectrum shows that there are water molecules in both **1** and **2** with absorptions of 3445 cm^{-1} and 3496 cm^{-1}, respectively (Fig. S2). The asymmetric and symmetric stretching of $—NO_2$ are assign to 1527 cm^{-1} and 1341 cm^{-1} for **1**, and these corresponding absorptions are 1531 cm^{-1} and 1347 cm^{-1} for **2** [23]. The asymmetric stretching adsorption band of COO^- are 1594 cm^{-1} for **1** and 1604 cm^{-1} for **2**, and the symmetric stretching adsorption band of COO^- are 1437 cm^{-1} for **1** and 1434 cm^{-1} for **2**, respectively [12,29]. The stretching vibrations of uranyl group are appear at 1084 cm^{-1}, 883 cm^{-1} and 817 cm^{-1} for **1**, and 1075 cm^{-1}, 930 cm^{-1} and 813 cm^{-1} for **2** [10,12,30]. Thermogravimetric curve measurements reveal the good thermostability of both **1** and **2**. Complex **1** mainly decompose at about 411 °C, complex **2**

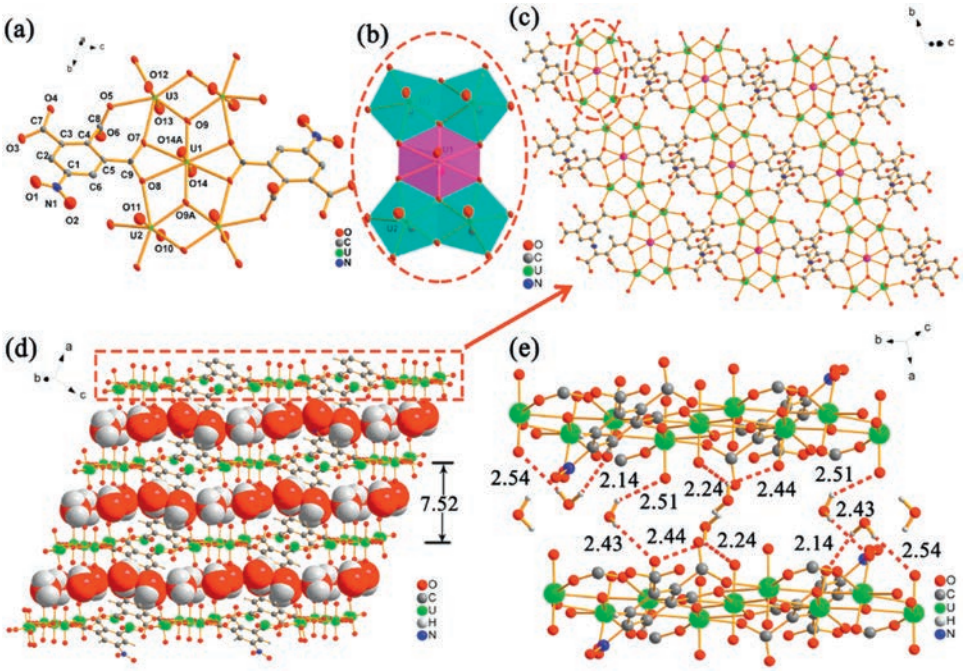

Fig. 1. Structural descriptions of **1**. (a) Coordination environment of the nbca ligand and uranyl centers. (b) The five uranyl polyhedron center unit structure. (c) The 2D sheer constructed from uranyl centers and nbca ligands. (d) Packing of the 2D sheer with the free water molecules imbedded. (e) The hydrogen bonds between adjacent layers.

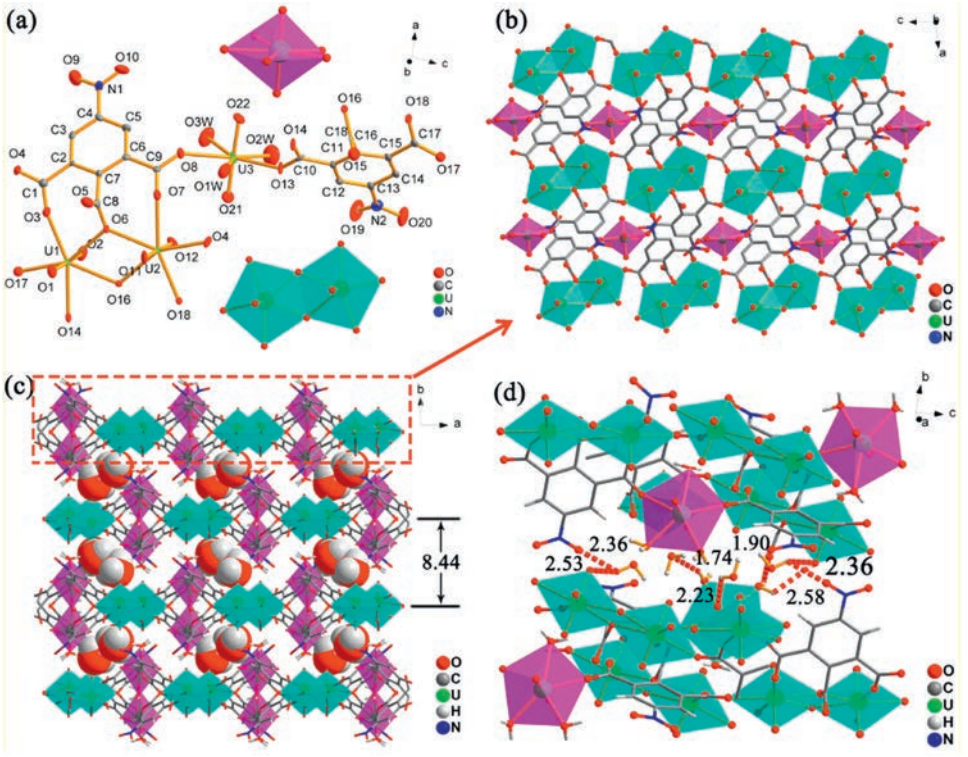

Fig. 2. Structural descriptions of **2**. (a) Coordination environment of the bpda ligand, the insert shows the decanedron geometry of U3 (purple) and the edge-sharing double decanedron geometry of U1 and U2 (blue). (b) The 2D layer net structure in ac plane of **2**. (c) Packing of the 2D layer with the interbeded free water viewed in ab plane. (d) The interbeded hydrogen bonds with H ··· A distances exhibited.

decompose at a higher temperature of about 426 °C. The first weight loss stage of about 5% and 6% are attributed to the water loss for **1** and **2**, respectively. There are both coordinated and free water in **2**, thus the weight loss curve of **2** appear steps (Fig. S5 in Supporting information).

The uranyl-bearing compounds usually demonstrate unique chare-transfer green emission with six characteristic peaks originated from the electronic and vibronic transitions S_{11}–S_{00} and S_{10}–$S_0\nu$ (ν = 0–4) of the UO_2^{2+} [25,31]. While complex **1** only exhibits a strong green emission at 547 nm (Fig. S6 in Supporting

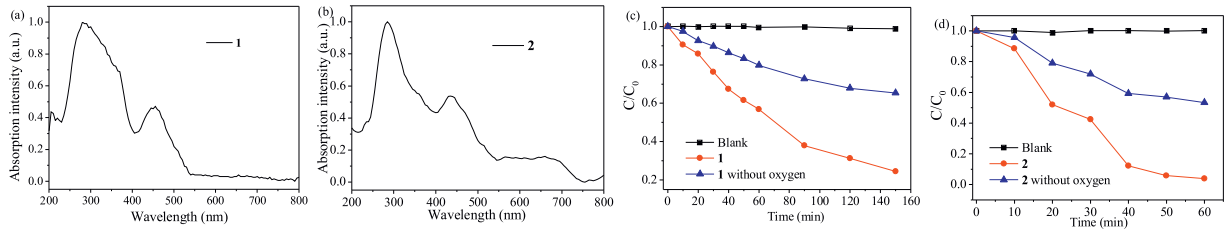

Fig. 3. UV – vis absorption spectra of (a) **1** and (b) **2**. Concentration change of RhB *versus* irradiation time of (c) **1** and (d) **2** in different conditions (*C* and C_0 represent the RhB concentrations after and before irradiation).

information). The emission spectrum of the pure nbca ligand shows a negligible emission peak centered at around 471 nm (Fig. S7 in Supporting information). We tentatively assign the emission of **1** to the ligand to metal electron charge transfer. The five uranyl membered center and the coordination of the nbca ligand may cause the overlap of the energy levels and change of electronic configuration [11], thus leading to the disappearing of the uranyl characteristic emission [30]. It has been reported that the structure and intensity of uranyl luminescence spectra depends on the bonding, symmetry and the local environment of UO_2^{2+}, not all of the uranyl compounds possess the six characteristic peaks [9,12,32]. Complex **2** exhibits five uranyl emission peaks at 498, 504, 520, 545 and 572 nm (Fig. 3). The maximum emission (520 nm) of **2** possesses 7 nm red shift compared to that of the benchmark compound $UO_2Ac_2{\cdot}2H_2O$ (Fig. S7). The coordination of the nbca ligand as well as the water molecules contribute together to the red shift of the emission of **2**.

The diffuse-reflectance UV/vis spectrum of complex **1** and **2** possess similar adsorption with strong adsorption at 285 nm ultraviolet regions and relatively weaker adsorption band at 455 nm for **1** and 435 nm for **2**, respectively (Fig. 4). The ultraviolet adsorption may attributed to the electronic charge-transfer transition from the doubly bonded O 2p bonding orbital to the nonbonding or antibonding orbitals of the uranyl group, while the visible component which responsible for color change is originated from ligand-to-metal charge transfer (LMCT) between the O atoms of the coordinated ligand and the empty orbital on the UVI ions [7,29]. The onsets (calculated by Kubelka–Munk function) of complex **1** and **2** appear at 2.46 eV and 2.43 eV, respectively (Fig. S8 in Supporting information). The visible-region charge-transfer transitions promoted us to explore the heterogeneous visible light photocatalysis applications for **1** and **2**.

A 300 W xenon lamp was used to simulate visible light irradiation to conduct the heterogeneous photocatalysis experiments. RhB, as a target pollutant for degradation experiments, was used here to evaluate the photocatalysis activity. As shown in the

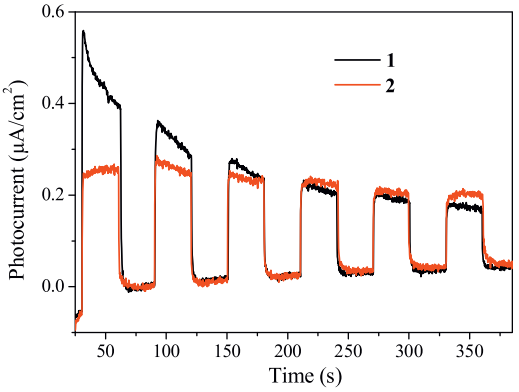

Fig. 4. The photoelectrochemical responses of **1** and **2** under visible light irradiation.

curves of RhB concentration *versus* irradiation time under different catalyzers (Figs. 4c and d). The RhB concentration kept nearly unchanged without the addition of uranyl complexes catalyzers, while decrease distinctly with adding of the uranyl complexes. 85.6% of RhB was degraded under photocatalysis of complex **1** in 150 min (Fig. 4c). The photocatalysis activity of **2** was obviously superior to that of **1** with about 96.2% of the RhB was degraded in only 60 min under catalysis of **2** (Fig. 4d). In order to examine the function of oxygen in the photocatalysis process, the photocatalysis activity of complexes **1** and **2** under anoxic conditions were evaluated. There are 65.3% of the RhB remained in the reaction system after irradiation of 150 min for **1** under anoxic condition and 53.4% remained after 60 min for **2**. It is obvious that the photocatalysis activity were reduced distinctly under anoxic condition.

In order to eliminate the adsorption of RhB by the complexes, we measured the time-dependent UV–vis adsorption spectra of the RhB solution within the complex samples in dark. As shown in Fig. S9 (Supporting information), the intensity of the UV–vis adsorption of RhB kept nearly unchanged in 50 min, which implies that the RhB adsorption by **1** and **2** are negligible surface adsorption. The powder XRD patterns before and after photocatalysis were nearly identical for **1** or **2**, which proved the excellent stability towards photocatalysis (Fig. S4). The photocurrent-time curves for **1** and **2** under irradiation of visible light are shown in Fig. 4. Both complexes exhibit typical on-off cycles of photocurrent. The photocurrent of **1** is stronger than **2** in the first three rounds. While the attenuation of **1** is more quickly than that of **2**, the photocurrent of **2** is relatively more stable than **1**, thus verified the better photocatalysis activity of **2** than **1** [33]. In addition, comparing to the five UO_8 centers constructed uranyl secondary building unit of **1**, the uranyl center in **2** takes coordination mode of UO_7 with potential unsaturated site which can approach RhB molecules in solution.

It has been proposed that hydrogen abstraction and electron transfer are the two mechanisms for the photocatalytic reactions involving uranyl [7]. Both the two ways originated from the excitation of uranyl, the excited $[UO_2^{2+}]^*$ which possess a high oxidation potential of 2.60 eV, is very active and can trigger a variety of redox reactions under the assistance of oxygen or H_2O_2 [9,12]. The uranyl center can be excited by photons with enough energy, during this process, electron jump from the HOMO orbitals of the bonded oxygen 2p to the LUMO of 5f uranium empty orbitals. The excited HOMO orbits are electron-withdrawing which can capture electrons form the RhB molecules with appropriate orientation in a reasonable range, resulting with the intermediate and hydrion [3,7]. The excited electron on the LUMO orbit may be captured by the oxygen in the solution forming highly active peroxide anion, which further oxidize and degrade the intermediates of RhB [7].

In conclusion, two 2D uranyl-carboxyl coordinated complexes **1** and **2**, which constructed from five membered UO_8 center SBUs and UO_7 molecular chains, respectively, were reported. Luminescence study reveals that the coordinated ligands may cause the

overlap of the energy levels thus resulting in disappearing or shifts of the uranyl characteristic emissions. Both **1** and **2** possess efficient photodegradation of RhB in aqueous solution, complex **2** exhibits fast photodegradation rate with 96.2% of the RhB degraded in only 60 min. The photocurrent measurements and contrast experiments in anoxic condition are performed to certify the mechanism. Our future work is to design and synthesis stable porous uranyl-based coordination polymers with dual-functions of absorption and photodegradation of dyes.

Declaration of competing interest

The authors report no declarations of interest.

Acknowledgments

The authors thank the support of National Science Foundations of China (No. 21461001), the Project of Jiangxi Provincial Department of Education (Nos. GJJ170436 and GJJ180367), the Natural Science Foundation of the Jiangsu Higher Education Institutions of China (No. 19JKB150007) and the Doctoral Scientific Research Foundation of East China University of Technology (No. DHBK2019143).

Appendix A. Supplementary data

Supplementary material related to this article can be found, in the online version, at doi:https://doi.org/10.1016/j.cclet.2020.11.044.

References

[1] E. Petrus, M. Segado, N.A.G. Bandeira, C. Bo, Inorg. Chem. 59 (2020) 8353–8360.
[2] J.T. Mayhugh, J.E. Niklas, M.G. Forbes, J.D. Gorden, A.E.V. Gorden, Inorg. Chem. 59 (2020) 9560–9568.
[3] X. Tong, S. Wang, H. Gao, et al., CrystEngComm 22 (2020) 5716–5722.
[4] J.G. Knapp, X. Zhang, T. Elkin, et al., CrystEngComm 22 (2020) 2097–2102.
[5] J. Xie, Y. Wang, W. Liu, et al., Angew. Chem. Int. Ed. 56 (2017) 7500–7504.
[6] P. Li, N.A. Vermeulen, X. Gong, et al., Angew. Chem. Int. Ed. 55 (2016) 1–6.
[7] Z.T. Yu, Z.L. Liao, Y.S. Jiang, G.H. Li, J.S. Chen, Chem. Eur. J. 11 (2005) 2642–2650.
[8] D. Wu, Y. Gao, W.G. Tian, et al., Chin. Chem. Lett. 27 (2016) 325–329.
[9] W. Xu, Z.X. Si, M. Xie, L.X. Zhou, Y.Q. Zheng, Cryst. Growth Des. 17 (2017) 2147–2157.
[10] J. Song, Y.H. Xing, X.M. Wang, et al., ChemistrySelect 1 (2016) 2316–2326.
[11] Z. Yue, J. Lin, M.A. Silver, et al., Dalton Trans. 47 (2018) 14908–14916.
[12] X.T. Xu, Y.N. Hou, S.Y. Wei, et al., CrystEngComm 17 (2015) 642–652.
[13] S.J. Jennifer, A.K. Jana, Cryst. Growth Des. 17 (2017) 5318–5329.
[14] P. Thuery, Y. Atoini, J. Harrowfield, Dalton Trans. 48 (2019) 8756–8772.
[15] S.W. An, L. Mei, K.Q. Hu, et al., Inorg. Chem. 59 (2020) 943–955.
[16] Y. Wang, Y. Li, Z. Bai, et al., Dalton Trans. 44 (2015) 18810–18814.
[17] L. Shao, F. Zhai, Y. Wang, et al., Dalton Trans. 48 (2019) 1595–1598.
[18] Q. Wang, Q. Gao, A.M. Al-Enizi, A. Nafady, S. Ma, Inorg. Chem. Front. 7 (2020) 300–339.
[19] Z.Q. Yao, G.Y. Li, J. Xu, T.L. Hu, X.H. Bu, Chem. Eur. J. 24 (2018) 3192–3198.
[20] W.W. He, N. Li, X. Wang, T.L. Hu, X.H. Bu, Chin. Chem. Lett. 29 (2018) 857–860.
[21] C.C. Wang, J.R. Li, X.L. Lv, Y.Q. Zhang, G. Guo, Energy Environ. Sci. 7 (2014) 2831–2867.
[22] X. Zhang, P. Li, M. Krzyaniak, et al., Inorg. Chem. 59 (2020) 16795–16798.
[23] X.S. Zhai, W.G. Zhu, W. Xu, Y.J. Huang, Y.Q. Zheng, CrystEngComm 17 (2015) 2376–2388.
[24] W. Yang, H. Wang, W.G. Tian, J. Li, Z.M. Sun, Eur. J. Inorg. Chem. 31 (2014) 5378–5384.
[25] W. Xu, Y.N. Ren, M. Xie, L.X. Zhou, Y.Q. Zheng, Dalton Trans. 47 (2018) 4236–4250.
[26] D. Sun, N. Zhang, Q.J. Xu, R.B. Huang, L.S. Zheng, Inorg. Chem. Commun. 13 (2010) 859–862.
[27] G.E. Gomez, J.A. Ridenour, N.M. Byrne, A.P. Shevchenko, C.L. Cahill, Inorg. Chem. 58 (2019) 7243–7254.
[28] L. Wang, W. Xu, W.Y. Li, M. Xie, Y.Q. Zheng, Chem. Asian J. 14 (2019) 4246–4254.
[29] W. Yang, W.G. Tian, X.X. Liu, L. Wang, Z.M. Sun, Cryst. Growth Des. 14 (2014) 5904–5911.
[30] X.X. Liu, Y. Wang, W.G. Tian, W. Yang, Z.M. Sun, Chin. Chem. Lett. 26 (2015) 641–645.
[31] P. Thuéry, Y. Atoini, J. Harrowfield, Cryst. Growth Des. 19 (2019) 6611–6626.
[32] P. Thuéry, Y. Atoini, J. Harrowfield, Cryst. Growth Des. 19 (2019) 4109–4120.
[33] S. Guo, Z. Deng, M. Li, et al., Angew. Chem. Int. Ed. 55 (2016) 1830–1834.